Science Advances
AAAS

advances.sciencemag.org/cgi/content/full/7/18/eabf9971/DC1

Supplementary Materials for

Toward a more sustainable mining future with electrokinetic in situ leaching

Evelien Martens, Henning Prommer*, Riccardo Sprocati, Jing Sun, Xianwen Dai, Rich Crane, James Jamieson, Pablo Ortega Tong, Massimo Rolle, Andy Fourie

*Corresponding author. Email: henning.prommer@csiro.au

Published 30 April 2021, *Sci. Adv.* **7**, eabf9971 (2021)
DOI: 10.1126/sciadv.abf9971

This PDF file includes:

Supplementary TextAnalytical Techniques

QXRD was used to determine the bulk mineralogy of the chalcopyrite specimen, as well as the crushed offcuts of the intact ore sample and the post-leaching ore sample. The QXRD analysis was carried out using a PANalytical Empyrean X-ray diffractometer with Cu Kα1 radiation equipped with a PIXcel detector. XRD data were interpreted with HighScore Plus (3.04) software using the ICDD database (2011).

The borate fusion method using lithium borate flux was used to prepare the crushed and milled offcuts from the intact ore sample as well as from the post-leaching ore sample for total elemental concentrations using ICP-OES.

Highly magnified images and high resolution compositional analysis of the crushed post-leaching ore sample were obtained using SEM-EDS. SEM-EDS analysis was conducted with a JEOL 7001F field emission scanning electron micro-analyzer equipped with a Bruker Esprit 1.9 EDS system using Bruker 10 mm SDD EDS detector with 125 eV resolution. The micro-analyzer was operated at an accelerating voltage of 20 kV, and a 10-mm working distance in backscattered electron imaging mode.

Nuclear magnetic resonance (NMR) was used to determine porosity and permeability of the intact ore. The NMR analysis was carried out with a GeoSpec 2 from Oxford-GIT Ltd. operated at 2.33 MHz on an offcut of the intact ore sample.

Dissolved Cu and Fe concentrations in all the solution samples were determined by an Agilent 240/280 atomic absorption spectrometer (AAS). The elemental compositions of some solution samples were also determined by ICP-OES. Accuracy of the AAS and ICP-OES analyses was verified against known quality controls. Dissolved Cu and Fe concentrations determined by AAS and ICP-OES were found to be consistent.

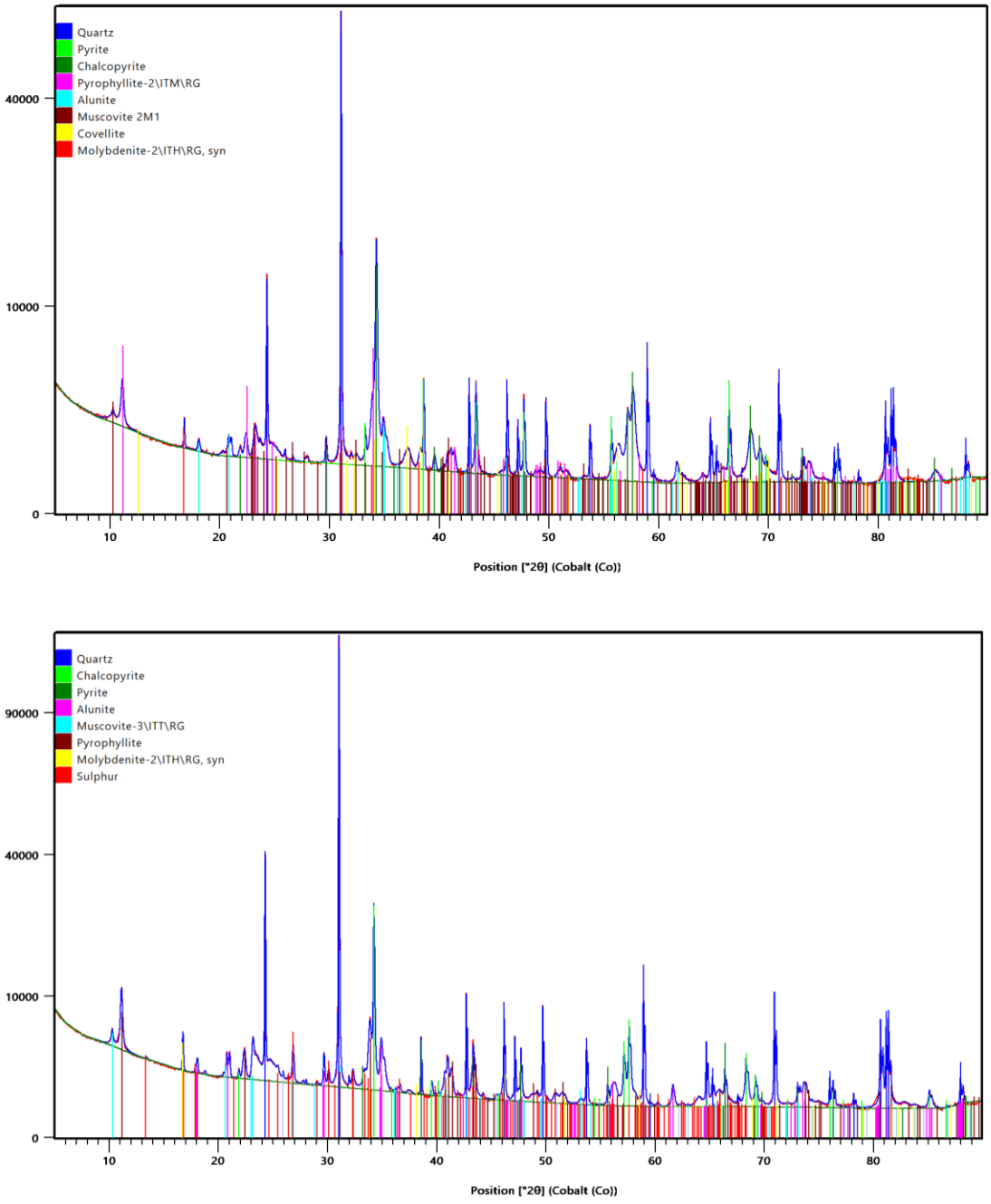

Fig. S1. XRD patterns and mineral phase identification of ore off-cut (Top) and ore sample after leaching by EK-ISL (Bottom). Quantification of mineralogical composition based on QXRD is provided in Table 3**.**

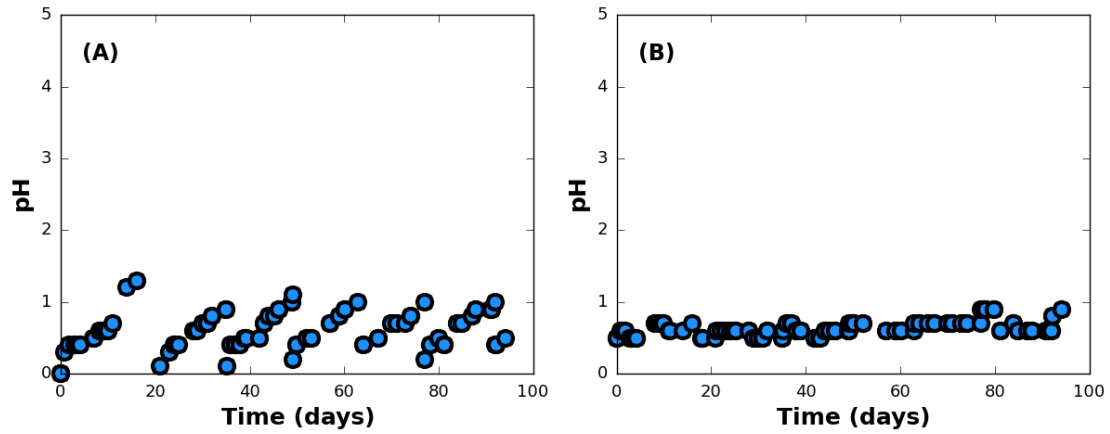

Fig. S2. Electrokinetic leaching of Cu from unfractured ore. pH in source (A) and target (B) as a function of time. The lixiviant in the source was refreshed on day 21, 35, 49, 63, 77 and 92. The target solution was renewed on day 7, 21, 35, 49, 63, 77 and 92.

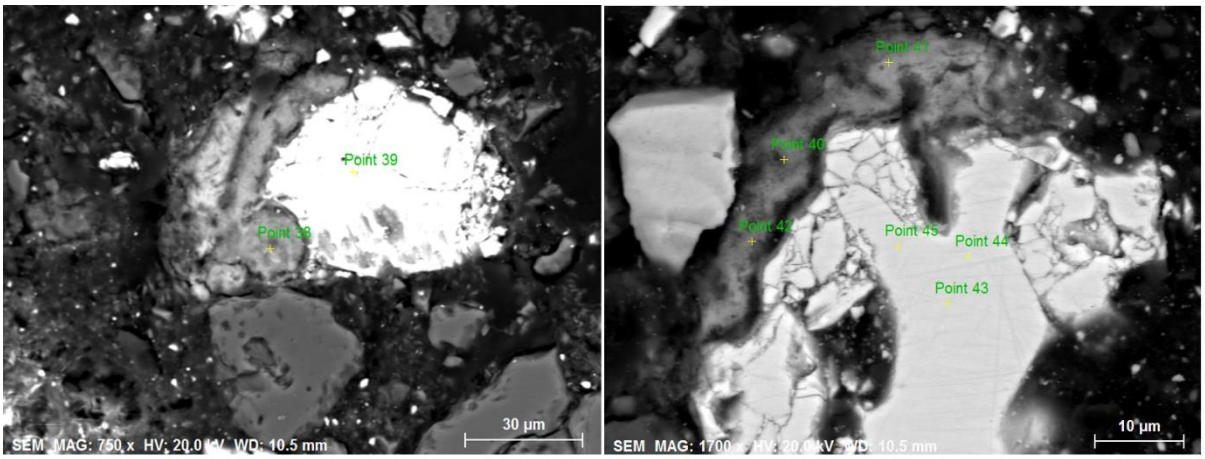

Fig. S3. SEM images of the intact copper ore sample, post EK-ISL leaching, showing the formation of elemental sulfur (light grey, points 38 and 40-42) associated with chalcopyrite (white area, points 39 and 43-45).

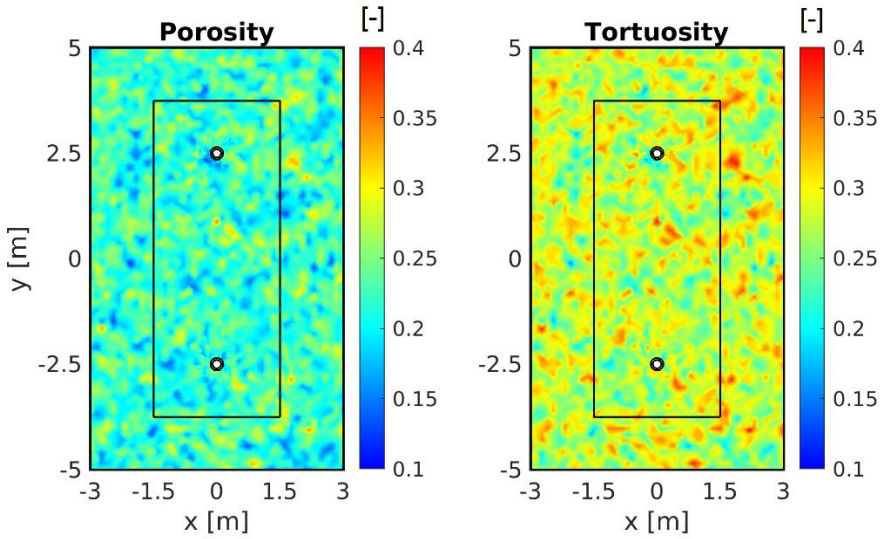

Fig. S4. Heterogeneous porosity (a) and tortuosity (b) distribution employed in the 2D field-scale simulation.

Table S1. Diffusion coefficients [m^2/s] of the modeled species at T=25 °C, from Lide (*55*).

Species	$\boldsymbol{D^{aq}}$
Na^+	1.33×10^{-9}
Cl^-	2.03×10^{-9}
Fe^{2+}	7.19×10^{-10}
Fe^{3+}	6.03×10^{-10}
Cu^{2+}	7.13×10^{-10}
H^+	9.31×10^{-9}
OH^-	5.27×10^{-9}

Table S2. Mineral amounts and composition.

Mineral amounts and composition	Units	Synthetic chalcopyrite and quartz model	Ore model
Unreactive fine quartz powder	g	360	-
Chalcopyrite powder	g	2	-
Chalcocite powder	g	0	-
Chalcopyrite	wt%	84.6	18.2
Chalcocite	wt%	0	0.8
Covellite	wt%	0	2.6
Chalcopyrite	g	1.692	19.82
Chalcocite	g	0	0.87
Covellite	g	0	2.83
Chalcopyrite	mmol	9.22	107.96
Chalcocite	mmol	0.00	5.47
Covellite	mmol	0.00	29.61
Amount of mineral per volume of solution			
Chalcopyrite	mM	80.98	22451.53
Chalcocite	mM	0.00	1138.05
Covellite	mM	0.00	6157.09

Table S3. Input model parameters for the 1-D laboratory experiments.

Input model parameters			
Parameter	Units	Synthetic chalcopyrite and quartz model	Ore model
ID		CP	Ore
Geometry type		Parallelepiped	Cylinder
Sample length	m	0.096	0.040
Sample width	m	0.0487	-
Sample height	m	0.0487	-
Sample transversal area	m2	2.37×10^{-3}	1.13×10^{-3}
Sample volume	m3	2.28×10^{-4}	4.54×10^{-5}
Average reservoir volume	L	0.42	0.42
Sample bulk density	kg/m^3	1800	2400
Sample mass	kg	0.41	0.109
Voltage at the Anode	V	12	5
Voltage at the Cathode	V	0	0
Distance between electrodes in the model	m	0.096	0.040
Electroosmotic coefficient	$m^2/(V\ s)$	0	0
Porosity	-	0.5	0.106
Tortuosity	-	0.5	0.3
Temperature	K	298	298
Total Simulation time	d	12	100
Renewal of solutions at the Source reservoir	d	0	0, 21, 35, 49, 63, 77, 92
Renewal of solutions at the Target reservoir	d	0	0, 7, 21, 35, 49, 63, 77, 92
Number of mesh elements	-	330	320

Table S4. Initial concentrations employed in the simulation of the 1-D laboratory experiments.

Initial concentrations			
Source reservoir (Anodic side)			
Na^{+}	mM	0	0
Cl^{-}	mM	470	800
Fe^{+3}	mM	90	200
H^{+}	mM	200	200
Target reservoir (Cathodic side)			
Na^{+}	mM	300	300
Cl^{-}	mM	500	500
Fe^{+3}	mM	0	0
H^{+}	mM	200	200
Concentration in the domain			
Na^{+}	mM	100	100
Cl^{-}	mM	100	100

Table S5. Calibrated rate constants for the simulation of the 1-D laboratory experiments.

Calibrated kinetic parameters			
k_{cp}	$mol^{-0.22}\ L^{0.22}/s$	150	2.00×10^{10}
a_{cp}	mol/L	50	8.00×10^{-1}
k_{pc}	1/s	-	1.00×10^{8}
a_{pc}	mol/L	-	1.00×10^{-4}

Table S6. Input model parameters for the 2D electrode pair model.

Input model parameters		
Parameter	Units	2D Electrode pair
Domain length	m	10
Domain width	m	6
Domain thickness	m	1
Domain volume	m^3	60
Inner domain height	m	7.5
Inner domain width	m	3
Inner domain thickness	m	1
Inner domain volume	m^3	22.5
Distance between electrodes	m	5
Electrode well diameter	m	0.2
Porosity range		0.09-0.33
Average porosity	-	0.22
Tortuosity range	-	0.14-0.41
Average tortuosity		0.28
Temperature	K	298
Voltage at the Anode	V	500
Voltage at the Cathode	V	0
Electroosmotic coefficient	$m^2/(V\ s)$	0
Total Simulation time	years	3
Bulk density	kg/m^3	2400
Inner domain weight	kg	54000
Number of mesh elements		6264

Table S7. Initial aqueous concentrations and mineral mass employed for the simulation of the 2D electrode pair model.

Initial concentrations		
Source reservoir (Anodic side)		
Na+	mM	0
Cl-	mM	800
Fe+3	mM	200
H+	mM	200
Target reservoir (Cathodic side)		
Na+	mM	300
Cl-	mM	500
Fe+3	mM	0
H+	mM	200
Background		
Na+	mM	100
Cl-	mM	100
Initial mineral mass		
Average amount of chalcopyrite per volume of solution	mM	760.00
Average mass of copper per volume of rock	kg/m3	11.00
Amount of copper (within chalcopyrite) in the inner domain	kg	611.99
Ore grade	wt% (Cu)	0.44

REFERENCES AND NOTES

1. D. Killick, T. Fenn, Archaeometallurgy: The study of preindustrial mining and metallurgy. *Ann. Rev. Anthropol.* **41**, 559–575 (2012).

2. M. Seredkin, A. Zabolotsky, G. Jeffress, In situ recovery, an alternative to conventional methods of mining: Exploration, resource estimation, environmental issues, project evaluation and economics. *Ore Geol. Rev.* **79**, 500–514 (2016).

3. M. Tayebi-Khorami, M. Edraki, G. Corder, A. Golev, Re-thinking mining waste through an integrative approach led by circular economy aspirations. *Minerals* **9**, 286 (2019).

4. B. Lottermoser, *Mine Wastes* (Springer Berlin Heidelberg, 2010); http://link.springer.com/10.1007/978-3-642-12419-8.

5. M. Azadi, S. A. Northey, S. H. Ali, M. Edraki, Transparency on greenhouse gas emissions from mining to enable climate change mitigation. *Nat. Geosci.* **13**, 100–104 (2020).

6. A. Fourie, Reflections on recent tailings dam failures and how the application of burland's soil mechanics triangle concept may avert future failures. *Geotech. Eng.* **51**, 60–64 (2020).

7. P. K. Robertson, D. J. Williams, G. Ward Wilson, *Report of the Expert Panel on the Technical Causes of the Failure of Feijão Dam I* (2019); http://b1technicalinvestigation.com/report.html.

8. N. R. Morgenstern, S. G. Vick, C. B. Viotti, B. D. Watts, *Report on the Immediate Causes of the Failure of the Fundão Dam* (2016); http://fundaoinvestigation.com/the-report/.

9. K. Hudson-Edwards, Tackling mine wastes. *Science* **352**, 288–290 (2016).

10. Wood Mackenzie, *Cobriza Copper Mine Report* (2020); https://woodmac.com/reports/metals-cobriza-copper-mine-16202151.

11. Newcrest Mining, *Market Release. Expert Review of Cadia Tailings Facility* (2019); https://newcrest.com/sites/default/files/2019-10/190430_Market Release_Expert review of Cadia tailings facility completed_0.pdf).

12. O. Vidal, B. Goffé, N. Arndt, Metals for a low-carbon society. *Nat. Geosci.* **6**, 894–896 (2013).

13. A. Elshkaki, T. E. Graedel, L. Ciacci, B. K. Reck, Copper demand, supply, and associated energy use to 2050. *Glob. Environ. Chang.* **39**, 305–315 (2016).

14. G. Calvo, G. Mudd, A. Valero, A. Valero, Decreasing ore grades in global metallic mining: A theoretical issue or a global reality? *Resources* **5**, 36 (2016).

15. K. D. Kelley, J. R. Lang, R. G. Eppinger, The giant Pebble Cu-Au-Mo deposit and surrounding region, southwest Alaska: Introduction. *Econ. Geol.* **108**, 397–404(2013).

16. R. A. Padilla Garza, S. R. Titley, F. Pimentel B, Geology of the escondida porphyry copper deposit, antofagasta Region, Chile. *Econ. Geol.* **96**, 307–324 (2001).

17. S. Northey, N. Haque, G. Mudd, Using sustainability reporting to assess the environmental footprint of copper mining. *J. Clean. Prod.* **40**, 118–128 (2013).

18. S. H. Ali, D. Giurco, N. Arndt, E. Nickless, G. Brown, A. Demetriades, R. Durrheim, M. A. Enriquez, J. Kinnaird, A. Littleboy, L. D. Meinert, R. Oberhänsli, J. Salem, R. Schodde, G. Schneider, O. Vidal, N. Yakovleva, Mineral supply for sustainable development requires resource governance. *Nature* **543**, 367–372 (2017).

19. C. Ferreira, P. Jensen, L. Ottosen, A. Ribeiro, Removal of selected heavy metals from MSW fly ash by the electrodialytic process. *Eng. Geol.* **77**, 339–347 (2005).

20. M. R. Jakobsen, J. Fritt-Rasmussen, S. Nielsen, L. M. Ottosen, Electrodialytic removal of cadmium from wastewater sludge. *J. Hazard. Mater.* **106**, 127–32 (2004).

21. Y. B. Acar, A. N. Alshawabkeh, Principles of electrokinetic remediation. *Environ. Sci. Technol.* **27**, 2638–2647 (1993).

22. R. Ortiz-Soto, D. Leal, C. Gutierrez, A. Aracena, A. Rojo, H. K. Hansen, Electrokinetic remediation of manganese and zinc in copper mine tailings. *J. Hazard. Mater.* **365**, 905–911 (2019).

23. R. F. Probstein, R. E. Hicks, Removal of contaminants from soils by electric fields. *Science* **260**, 498–503 (1993).

24. R. H. Sillitoe, Porphyry copper systems. *Econ. Geol.* **105**, 3–41 (2010).

25. L. Sinclair, J. Thompson, In situ leaching of copper: Challenges and future prospects. *Hydrometallurgy* **157**, 306–324 (2015).

26. R. D. Schmidt, D. Earley, M. J. Friedel, *In Situ Recovery of Minerals II. Engineering Foundation*, S. A. Swan, K. R. Coyne, Eds. (TMS, The metals, minerals and materials society, 1994), pp. 259–288.

27. J. E. Dutrizac, Elemental sulphur formation during the ferric chloride leaching of chalcopyrite. *Hydrometallurgy* **23**, 153–176 (1990).

28. G.-N. Kim, D.-B. Shon, H.-M. Park, K.-W. Lee, U.-S. Chung, Development of pilot-scale electrokinetic remediation technology for uranium removal. *Sep. Purif. Technol.* **80**, 67–72 (2011).

29. E. Mena, J. Villaseñor, M. A. Rodrigo, P. Cañizares, Electrokinetic remediation of soil polluted with insoluble organics using biological permeable reactive barriers: Effect of periodic polarity reversal and voltage gradient. *Chem. Eng. J.* **299**, 30–36 (2016).

30. D. Hodges, A. Fourie, D. Thomas, D. Reynolds, Overcoming permanganate stalling during electromigration. *J. Environ. Eng.* **139**, 677–684 (2013).

31. S. S. Kim, S. J. Han, Application of an enhanced electrokinetic ion injection system to bioremediation. *Water Air Soil Pollut.* **146**, 365–377 (2003).

32. C. A. J. Appelo, Solute transport solved with the Nernst-Planck equation for concrete pores with 'free' water and a double layer. *Cem. Concr. Res.* **101**, 102–113 (2017).

33. D. A. Singer, V. I. Berger, B. C. Moring, *Porphyry Copper Deposits of the World: Database, Maps, and Preliminary Analysis* (U.S. Geological Survey, 2002); https://pubs.er.usgs.gov/publication/ofr02268.

34. R. Sprocati, M. Masi, M. Muniruzzaman, M. Rolle, Modeling electrokinetic transport and biogeochemical reactions in porous media: A multidimensional Nernst–Planck–Poisson approach with PHREEQC coupling. *Adv. Water Resour.* **127**, 134–147 (2019).

35. R. Sprocati, M. Rolle, Charge interactions, reaction kinetics and dimensionality effects on electrokinetic remediation: A model-based analysis. *J. Contam. Hydrol.* **229**, 103567 (2020).

36. M. André, M. E. Malmström, I. Neretnieks, Determination of sorption properties of intact rock samples: New methods based on electromigration. *J. Contam. Hydrol.* **103**, 71–81 (2009).

37. M. Löfgren, I. Neretnieks, Through-electromigration: A new method of investigating pore connectivity and obtaining formation factors. *J. Contam. Hydrol.* **87**, 237–252 (2006).

38. E. Puukko, J. Lehto, A. Lindberg, M. Voutilainen, Electromigration experiments for studying transport parameters and sorption of cesium and strontium on intact crystalline rock. *J. Contam. Hydrol.* **217**, 1–7 (2018).

39. R. W. Bartlett, *Solution Mining: Leaching and Fluid Recovery of Minerals* (Routledge, ed. 2, 1998).

40. E. Martens, H. Prommer, X. Dai, J. Sun, P. Breuer, A. Fourie, Electrokinetic in situ leaching of gold from intact ore. *Hydrometallurgy.* **178**, 124–136 (2018).

41. M. M. Antonijević, G. D. Bogdanović, Investigation of the leaching of chalcopyritic ore in acidic solutions. *Hydrometallurgy* **73**, 245–256 (2004).

42. C. R. Bennett, D. McBride, M. Cross, J. E. Gebhardt, A comprehensive model for copper sulphide heap leaching: Part 1 Basic formulation and validation through column test simulation. *Hydrometallurgy* **127–128**, 150–161 (2012).

43. N. Hiroyoshi, M. Arai, H. Miki, M. Tsunekawa, T. Hirajima, A new reaction model for the catalytic effect of silver ions on chalcopyrite leaching in sulfuric acid solutions. *Hydrometallurgy*. **63**, 257–267 (2002).

44. E. Martens, H. Prommer, X. Dai, M. Z. Wu, J. Sun, P. Breuer, A. Fourie, Feasibility of electrokinetic in situ leaching of gold. *Hydrometallurgy* **175**, 70–78 (2018).

45. D. Hodges, A. Fourie, D. Reynolds, D. Thomas, *Development of An Apparatus for pH-isolated Electrokinetic In Situ Chemical. J. Environ. Eng.* **137**, 809–816 (2011).

46. J. Newman, K. E. Thomas-Alyea, *Electrochemical Systems* (John Wiley & Sons, 2004).

47. A. D. MacGillivray, Nernst-Planck equations and the electroneutrality and Donnan equilibrium assumptions. *J. Chem. Phys.* **48**, 2903–2907 (1968).

48. M. Sastre, J. A. Santaballa, A note on the meaning of the electroneutrality condition for solutions. *J. Chem. Educ.* **66**, 403 (1989).

49. B. E. Kimball, J. D. Rimstidt, S. L. Brantley, Chalcopyrite dissolution rate laws. *Appl. Geochem.* **25**, 972–983 (2010).

50. N. N. Saxena, N. R. Mandre, Mixed control kinetics of copper dissolution for copper ore using ferric chloride. *Hydrometallurgy* **28**, 111–117(1992).

51. C. Y. Cheng, F. Lawson, The kinetics of leaching chalcocite in acidic oxygenated sulphate-chloride solutions. *Hydrometallurgy* **27**, 249–268 (1991).

52. S. Müller, L. Schüler, *GeoStat-Framework/GSTools: Reverberating Red (Version v1.1.0)* (Zenodo, 2019); http://doi.org/10.5281/zenodo.3468230.

53. J. Cai, W. Wei, X. Hu, D. A. Wood, Electrical conductivity models in saturated porous media: A review. *Earth Sci. Rev.* **171**, 419–433 (2017).

54. D. L. Parkhurst, L. Wissmeier, PhreeqcRM: A reaction module for transport simulators based on the geochemical model PHREEQC. *Adv. Water Resour.* **83**, 176–189 (2015).

55. D. R. Lide, *CRC Handbook of Chemistry and Physics* (CRC, London, ed. 84, 2003).